

Robust Multiview Point Cloud Registration with Reliable Pose Graph Initialization and History Reweighting

Haiping Wang*
Wuhan University

Yuan Liu*
The University of Hong Kong

Zhen Dong†
Wuhan University

Yulan Guo
Sun Yat-sen University

Yu-Shen Liu
Tsinghua University

Wenping Wang
Texas A&M University

Bisheng Yang†
Wuhan University

Abstract

In this paper, we present a new method for the multiview registration of point cloud. Previous multiview registration methods rely on exhaustive pairwise registration to construct a densely-connected pose graph and apply Iteratively Reweighted Least Square (IRLS) on the pose graph to compute the scan poses. However, constructing a densely-connected graph is time-consuming and contains lots of outlier edges, which makes the subsequent IRLS struggle to find correct poses. To address the above problems, we first propose to use a neural network to estimate the overlap between scan pairs, which enables us to construct a sparse but reliable pose graph. Then, we design a novel history reweighting function in the IRLS scheme, which has strong robustness to outlier edges on the graph. In comparison with existing multiview registration methods, our method achieves 11% higher registration recall on the 3DMatch dataset and $\sim 13\%$ lower registration errors on the ScanNet dataset while reducing $\sim 70\%$ required pairwise registrations. Comprehensive ablation studies are conducted to demonstrate the effectiveness of our designs. The source code is available at <https://github.com/WHU-USI3DV/SGHR>.

1. Introduction

Point cloud registration is a prerequisite for many tasks such as 3D reconstruction [17, 25, 32] and 3D segmentation [27, 35]. Most recent registration methods [1, 7, 22, 28, 39, 46, 49, 57] mainly focus on pairwise registration of two partial point clouds (scans), which can only reconstruct a part of the scene. In order to get a completed scene recon-

*Both authors contribute equally to this research.

†Corresponding authors: [dongzhenwhu, bshyang]@whu.edu.cn

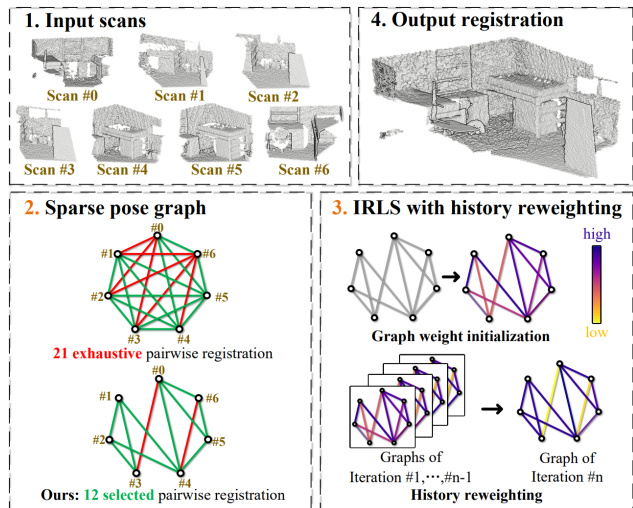


Figure 1. **Overview.** (1) Given N unaligned partial scans, our target is to register all these scans into (4) a completed point cloud. Our method has two contributions. (2) We learn a global feature vector to initialize a sparse pose graph which contains much less outliers and reduces the required number of pairwise registrations. (3) We propose a novel IRLS scheme. In our IRLS scheme, we initialize weights from both global features and pairwise registrations. Then, we design a history reweighting function to iteratively refine poses, which improves the robustness to outliers.

struction, all partial point clouds should be simultaneously aligned, which is called *multiview registration*. Due to its complexity, multiview point cloud registration receives less attention recently and only few recent studies propose multiview registration methods [18, 21, 30, 54, 55].

Given N unaligned partial point clouds, multiview registration aims to find a globally-consistent pose for every partial point cloud. A commonly-adopted pipeline of multiview registration consists of two phases [55]. First, a pairwise registration algorithm [28, 46, 49] is applied to ex-

haustively estimate the relative poses of all $\binom{N}{2}$ scan pairs, which forms a fully-connected pose graph. The edges of the graph stand for the relative poses of scan pairs while nodes represent scans. Since the dense pose graph may include inaccurate or even incorrect relative poses (outliers) between two irrelevant scans, in the second phase, these pairwise poses are jointly optimized by enforcing the cycle consistency [30] to reject outlier edges and improve accuracy. For the second phase, most recent methods, including hand-crafted methods [5, 13, 29] or learning-based [21, 30, 55] methods, follow a scheme of Iterative Reweighting Least Square (IRLS). In the IRLS, initial weights are assigned to edges to indicate these edges are reliable or not. Then, based on the weights, a synchronization algorithm is applied to compute a new relative pose on every edge. After that, the weights on edges are updated according to the difference between the old relative poses and the new ones. IRLS iteratively synchronize poses from edge weights and update weights with synchronized poses.

In an ideal case, an IRLS scheme will gradually lower the weights of the outlier edges and only consider the inlier edges for pose synchronization. However, the initial densely-connected graph contains lots of outliers, which often prevents the iterative reweighting mechanism of IRLS from finding correct edges. To improve the robustness to outliers, many researches focus on applying advanced hand-crafted reweighting functions [11, 29] or designing graph network to learn reweighting functions [30, 55]. However, the handcrafted reweighting functions usually require a good initialization to converge to the correct poses while learning-based reweighting methods may not generalize to unseen settings. Designing a robust IRLS algorithm still remains an open problem.

In this paper, we show that multiview registration can be improved from two aspects, as shown in Fig. 1. First, we learn a good initialization of the input pose graph which avoids exhaustive pairwise registrations and reduces the outlier ratio. Second, we propose a novel history reweighting function which enables a stable convergence to correct poses in the IRLS scheme.

In the pose graph construction, we learn a global feature on each point cloud and the correlation of two global feature indicates the overlap ratio between two point clouds. Such global features enable us to generate a sparse pose graph with fewer but more reliable edges instead of a densely-connected graph. After that, we only need to apply the pairwise registration algorithm and IRLS on these sparse edges, which greatly reduce the computation complexity of pairwise registration from $O(N^2)$ to $O(N)$. Meanwhile, these reliable edges contain much less outliers than the fully-connected graph, which provides the possibility to find more accurate and consistent global poses in IRLS.

Though the initial graph contains much less outliers, ex-

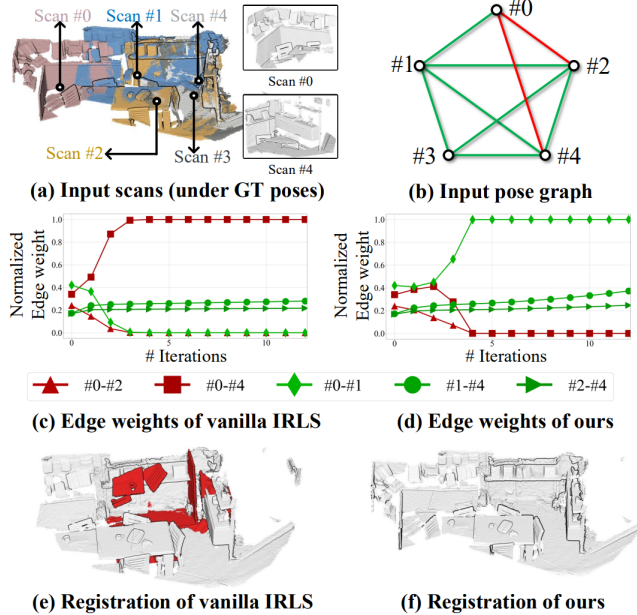


Figure 2. An example on the 3DMatch dataset. (a) The input scans under the ground truth poses. (b) The constructed sparse pose graph with two incorrect relative poses (#0-#2 and #0-#4), where #0 and #4 looks very similar to each other so that the pose graph incorrectly include this scan pair. (c) and (d) show the normalized weights on the graph edges on different iterations of the vanilla IRLS and our method respectively. Our method is able to find the outlier edges and gradually reduce their weights while vanilla IRLS is biased towards the outlier edge (#0-#4) after few iterations. (e) and (f) are the multiview registration results of the vanilla IRLS and our method respectively.

isting IRLS algorithms are still sensitive to these outliers and can be totally biased towards these outliers in the first few iterations. An example is shown in Fig. 2: the initial graph only contains two outlier edges. However, the outlier scan pair “#0-#4” looks very similar and thus is initialized with a large weight. Such an incorrect large weight interferes the subsequent pose synchronization and brings systematic errors to the synchronized poses. The vanilla IRLS trusts all synchronized poses and is easily dominated by these erroneous poses, which leads to incorrect convergence as shown in Fig. 1(c). To address this problem, we propose a simple yet effective reweighting function called the *history reweighting function*. In history reweighting function, edge weights at a specific iteration not only depends on the synchronized poses at the current iterations but also considers the historical synchronized poses in previous iterations, which acts like a regularizer to prevent the IRLS from being dominated by outliers at the early unstable iterations as shown in the Fig. 2 (d). Then, the edge weights in our graph gradually stabilize in the subsequent iterative refinements, leading to the convergence to correct poses.

We evaluate our method on three widely-used benchmarks: the 3DMatch/3DLoMatch dataset [28, 59], the ScanNet dataset [16], and the ETH dataset [44]. With the help of the proposed sparse graph construction and IRLS with history reweighting, our method surpasses the current multiview registration baselines by 11.0% and 6.2% in registration recall on 3DMatch and 3DLoMatch, reduces the mean rotation and translation errors on ScanNet by 12.8% and 13.8%. Meanwhile, our method shows strong generalization ability. Only trained on the indoor dataset, our method achieves a 99.8% registration recall on the outdoor ETH dataset. Moreover, all the above state-of-the-art performances of our method only require 20% ~ 40% pairwise registrations of existing multiview point cloud registration methods, which demonstrates our computation efficiency.

2. Related work

2.1. Pairwise registration

There are mainly two kinds of pairwise point cloud registrations. Feature-based methods extract a set of local descriptors [1, 7, 15, 22, 49, 50] on detected keypoints [7, 28]. Then, local descriptors are matched to build correspondences [39, 46, 56, 57]. Finally, correspondences are filtered [6, 12, 14, 36, 43] and used in transformation estimation [46, 49, 56] to find rigid transformations. Other works, known as direct registration methods, either directly regress the transformations [2, 31, 38, 58] or refine correspondences [20, 40, 51, 52] by considering the information from both point clouds with attention layers. Our multiview registration method is based on the pairwise registration, which is compatible with all above methods.

2.2. Multiview registration

Most multiview point cloud registration methods [5, 10, 13, 19, 21, 23, 29, 30, 55] aim at recovering the absolute scan poses from exhaustive pairwise registrations. However, exhaustive pairwise registration is time-consuming [18] and may contain lots of outliers [55]. To reduce the computational burden, some traditional works [18, 24, 33, 42, 53] resort to growing-based strategy to merge selected scans iteratively, which requires fewer pairwise registrations but may fail due to the accumulated errors in the growing process. In contrast, we avoid complex growing strategies to find inlier pairs but incorporate learning-based techniques to select reliable scan pairs, which enables more accurate subsequent synchronization. Other works [5, 9, 13, 21, 30, 33, 47, 48, 55, 60] focus on pruning outliers on the constructed graph. IRLS-based scheme is one of the most prevalent technique [5, 8, 21, 26, 29, 30, 55]. However, the iterative refinement of IRLS can easily be trapped in a local minima and fails to prune out outlier edges [5, 55]. The reweighting function is proved to be the most important design in a

reliable IRLS [5, 26, 30]. Thus, recent learning-based advances [21, 30, 55] adopt data-driven strategy to learn robust reweighting functions, which achieve impressive performances but cannot generalize well to unfamiliar graphs. We design a history reweighting function with strong generalization ability and robustness to outliers.

3. Method

3.1. Overview

Consider a set of unaligned scans $\mathcal{P} = \{P_i | i = 1, \dots, N\}$ in the same 3D scene. The target of multiview registration is to recover the underlying global scan poses $\{T_i = (R_i, t_i) \in SE(3) | i = 1, \dots, N\}$. In the following, we first introduce how to initialize a pose graph with reliable edges in Sec. 3.2. Then, we propose a novel history reweighting function within a IRLS scheme in Sec. 3.3 to solve for the poses of every scan. The pipeline is illustrated in Fig. 3.

3.2. Learn to construct a sparse graph

In this section, we aim to construct a pose graph for the multiview registration. Specifically, the graph is denoted by $\mathcal{G}(\mathcal{V}, \mathcal{E})$, where each vertex $v_i \in \mathcal{V}$ represents each scan P_i while edge $(i, j) \in \mathcal{E}$ encodes the relative poses between scan P_j and scan P_i . We will first estimate an overlap score s_{ij} for each scan pair (P_i, P_j) . Then, given the overlap scores, we construct a sparse graph by selecting a set of scan pairs with large estimated overlaps and apply pairwise transformations on them only.

Global feature extraction. To extract the global feature F for a point cloud P , we first downsample P by voxels and extract a local feature $f_p \in \mathbb{R}^d$ on every sampled point $p \in P$ from its local 3D patch $N_p = \{p' | \|p - p'\|_2 < r, p' \in P\}$ within a radius of r by

$$f_p = \varphi(N_p), \quad (1)$$

where φ is a neural network for extracting local descriptors, such as PointNet [45], FCGF [15], and YOHO [49]. By default, we adopt YOHO as the local descriptor [49] due to its superior performance. Then, we apply a NetVLAD [3] layer on the local features to extract a global feature F

$$F = \text{NetVLAD}(\{f_p\}). \quad (2)$$

Note $F \in \mathbb{R}^n$ is normalized such that $\|F\|_2 = 1$.

Sparse graph construction. For a scan pair (P_i, P_j) , we estimate their overlap score by

$$s_{ij} = (F_i^T F_j + 1)/2, \quad (3)$$

where $s_{ij} \in [0, 1]$ indicates the overlap between P_i and P_j . We train the *NetVLAD* with a L1 loss between the predicted overlap score and the ground-truth overlap ratio.



Figure 3. The pipeline of the proposed method.

For each scan, we select other k scan pairs with the largest overlap scores to connect with the scan. This leads to a sparse graph with edges

$$\mathcal{E} = \{(i, j : \arg\text{-topk } s_{ij}), \forall P_i \in \mathcal{P}\}. \quad (4)$$

On each edge $(i, j) \in \mathcal{E}$ of the constructed graph, we estimate a relative pose T_{ij} on the scan pair from their extracted local descriptors. By default, we follow [49] to apply nearest neighborhood matcher on the local descriptors and estimate the relative pose from the RANSAC variant.

Discussion. Recent multiview registration methods [21, 30, 55, 60] usually exhaustively estimate all $\binom{N}{2}$ relative poses and many of these scan pairs have no overlap at all. In our method, we extract global features to determine the overlap scores to select $N \times k$ scan pairs. Actually, we only need to conduct pairwise registration less than $N \times k$ because the graph is an indirection graph and we only need to count each edge once. Our global feature extraction is much more efficient than matching descriptors and running RANSAC in the pairwise registration. The subsequent pose synchronization only needs to operate on these sparse edges, which also improves the efficiency. Moreover, the retained pose graph contains much less fewer outliers, which thus improves the accuracy of the subsequent synchronization.

3.3. IRLS with history reweighting

In this section, we apply the Iteratively Reweighted Least Squares (IRLS) scheme to estimate the consistent global poses on all scans. The key idea of IRLS is to associate a weight on each edge to indicate the reliability of each scan pair. These weights are iteratively refined such that outlier edges will have small weights so these outlier relative poses will not affect the final global poses. In the following, we first initialize edge weights, and iteratively estimate poses based on edge weights and update edge weights with the proposed history reweighting function.

3.3.1 Weight initialization

The weight $w_{ij}^{(0)}$ is initialized from both the estimated overlap score s_{ij} and the quality of the pairwise registration by

$$w_{ij}^{(0)} = s_{ij} * r_{ij}, \quad (5)$$

where r_{ij} reveals the quality of pairwise registration. In the pairwise registration, a set of correspondences $C = \{(p, q) | p \in P_i, q \in P_j\}$ are established by matching local descriptors. Thus, r_{ij} is defined as the number of inlier correspondences in C conforming with $T_{ij} = (R_{ij}, t_{ij})$, which is

$$r_{ij} = \sum_{(p,q) \in C} [\|p - R_{ij}q - t_{ij}\|^2 < \tau], \quad (6)$$

where $[\cdot]$ is the Iverson bracket, τ is a pre-defined inlier threshold.

3.3.2 Pose synchronization

Given the edge weights and input relative poses $\{w_{ij}, T_{ij} = (R_{ij}, t_{ij}) | (i, j) \in \mathcal{E}\}$, we solve for the global scan poses $\{T_i = (R_i, t_i)\}$. We adopt the closed-form synchronization algorithm proposed in [4, 30]. We first compute the rotations by rotation synchronization [4, 21], and then compute the translations by translation synchronization [30].

Rotation synchronization. The goal of rotation synchronization is to solve

$$\{R_1, \dots, R_N\} = \arg \min_{R_1, \dots, R_N \in SO(3)} \sum_{(i,j) \in \mathcal{E}} w_{ij} \|R_{ij} - R_i^T R_j\|_F^2, \quad (7)$$

where $\|\cdot\|_F$ means the Frobenius norm of the matrix. The problem has a closed-form solution, which can be derived from the eigenvectors of a symmetric matrix $L \in \mathbb{R}^{3N \times 3N}$

$$L = \begin{pmatrix} \sum_{(1,j) \in \mathcal{E}} w_{1j} \mathbf{I}_3 & -w_{12} R_{12} & \cdots & -w_{1N} R_{1N} \\ -w_{21} R_{21} & \sum_{(2,j) \in \mathcal{E}} w_{2j} \mathbf{I}_3 & \cdots & -w_{2N} R_{2N} \\ \vdots & \vdots & \ddots & \vdots \\ -w_{N1} R_{N1} & -w_{N2} R_{N2} & \cdots & \sum_{(N,j) \in \mathcal{E}} w_{Nj} \mathbf{I}_3 \end{pmatrix} \quad (8)$$

L is a sparse matrix since the constructed graph is sparse. Given three eigenvectors $\tau_1, \tau_2, \tau_3 \in \mathbb{R}^{3N}$ corresponding to the three smallest eigenvalues $\lambda_1 < \lambda_2 < \lambda_3$ of L , we stack these three eigenvectors to construct a matrix $V = [\tau_1, \tau_2, \tau_3] \in \mathbb{R}^{3N \times 3}$. Then, R_i can be derived by projecting

$v_i = V[3i - 3 : 3i] \in \mathbb{R}^{3 \times 3}$ to $SO(3)$. More details can be found in the supplementary material.

Translation synchronization. Similarly, translation synchronization retrieves the translation vectors $\{t_i\}$ that minimize the problem:

$$\{t_1, \dots, t_N\} = \arg \min_{t_1, \dots, t_N \in \mathbb{R}^3} \sum_{(i,j) \in \mathcal{E}} w_{ij} \|R_i t_{ij} + t_i - t_j\|^2 \quad (9)$$

We solve it by the standard least square method [30].

3.3.3 History reweighting function

Given the synchronized poses, we re-compute weights on edges such that outlier edges will have smaller weights than the inlier edges. Assume the synchronized poses at the n -th iteration are $\{T_i^{(n)} = (R_i^{(n)}, t_i^{(n)})\}$. We first compute the rotation residual $\delta_{ij}^{(n)}$ by

$$\delta_{ij}^{(n)} = \Delta(R_{ij}, R_i^{(n)T} R_j^{(n)}), \quad (10)$$

where $\Delta(R_1, R_2)$ means the angular difference between the rotation R_1 and R_2 . $\Delta(R_1, R_2)$ is implemented by transforming $R_1^T R_2$ into an axis-angle form and outputting the rotation angle. Then, the updated weights are computed from rotation residuals of all previous iterations by

$$w_{ij}^{(n)} = w_{ij}^{(0)} \exp\left(-\sum_{m=1}^n g(m) \delta_{i,j}^{(m)}\right), \quad (11)$$

where $g(m)$ is a predefined coefficient function of the iteration number with $g(m) > 0$. We will elaborate the design of $g(m)$ later. Instead, we first discuss the intuition behind the Eq. (11).

Intuition of Eq. (11). Similar to previous reweighting functions [5, 21, 55], a larger rotation residual δ will lead to a smaller weight because large residuals are often caused by outliers. Meanwhile, there are two differences from previous reweighting functions. First, we multiply the initial weights $w_{ij}^{(0)}$ so that the recomputed weights always retain information from the warm-start initialization in Sec. 3.3.1 and these initialized weights will be adjusted by the residuals in the iterative refinement. Second, the weight at a specific iteration n considers the residuals of all previous iterations $m \leq n$. This design is inspired from the momentum optimization method RMSProp or Adam [34], which utilizes the gradients in the history to stabilize the optimization process. Here, we adopt similar strategy to consider all residuals in the history to determine a robust weight for the current iteration, which is less sensitive to outliers.

Design of coefficient function $g(m)$. $g(m)$ can be regarded as a weight function. A small value of $g(m)$ means that we do not trust the residual at the iteration m and

this residual may not correctly identify inliers and outliers. In our observation, the residuals estimated by the first few iterations are not very stable so we want $g(m)$ is increasing with the iteration number m . Meanwhile, if we want to conduct M IRLS iterations in total, we want the sum of coefficients at the final iteration M will be 1, i.e. $\sum_{m=1}^M g(m) = 1$. Thus, in our design, we have

$$g(m) = \frac{2m}{M(M+1)}. \quad (12)$$

After computing the updated weights, we iteratively synchronize the poses with these updated weights as stated in Sec. 3.3.2 and compute new weights from these new poses as stated in Sec. 3.3.3. The IRLS run M iterations in total and the synchronized poses at the final iteration are regarded as the output poses for all scans.

4. Experiments

4.1. Experimental protocol

4.1.1 Datasets

We evaluate the proposed method on three widely used datasets: 3D(Lo)Match [28, 59], ScanNet [16], and ETH [44] as follows.

3DMatch contains scans collected from 62 indoor scenes among which 46 are split for training, 8 for validation, and 8 for testing. Each test scene contains 54 scans on average. We follow previous works [21, 28] to use 1623 scan pairs with $> 30\%$ overlap ratio and 1781 scan pairs with $10\% \sim 30\%$ overlap as two test sets, denoted as 3DMatch and 3DLoMatch, respectively.

ScanNet contains RGBD sequences of 1513 indoor scenes. We follow [21] to use the same 32 test scenes and convert 30 RGBD images that are 20 frames apart to 30 scans on each scene. There are 960 scans in total and we exhaustively select all 13920 scan pairs for evaluation.

ETH has 4 outdoor scenes with large domain gaps to the 3DMatch dataset and each scene contains 33 scans on average. 713 scan pairs are officially selected for evaluation.

Our model is only trained on the training split of 3DMatch and evaluated on 3D(Lo)Match, ScanNet, and ETH. More training details can be found in supplementary material. For evaluation, we first perform multiview registration to recover the global scan poses. Then, we follow [21] to evaluate the multiview registration quality on pairwise relative poses computed from the recovered global poses. By default, we set k in sparse graph construction to 10 for two indoor datasets and 6 for the ETH dataset.

4.1.2 Metrics

We follow [1, 15, 46, 49] to adopt Registration Recall (RR) for evaluation on 3D(Lo)Match and ETH. RR reports the

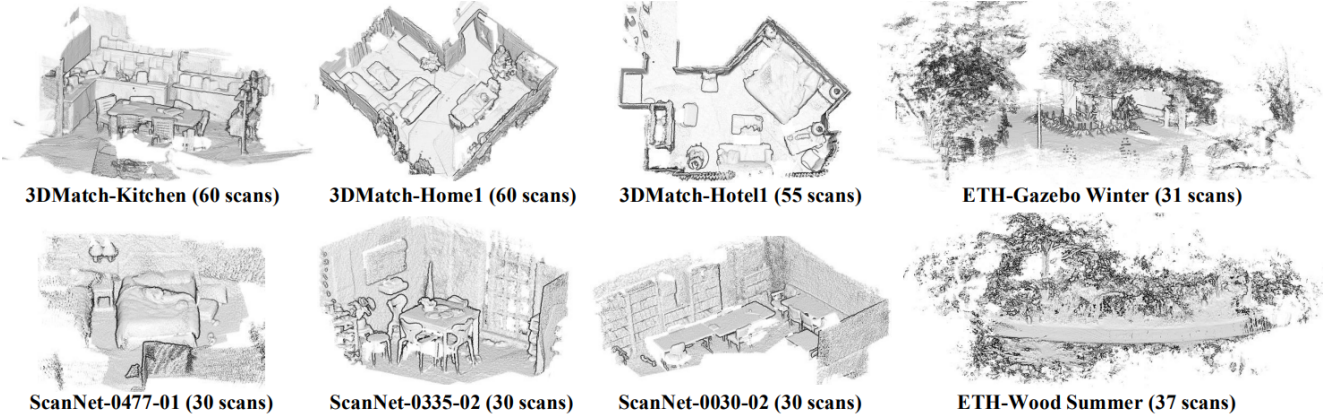


Figure 4. Qualitative results on the 3DMatch, ScanNet, and ETH datasets.

ratio of correctly aligned scan pairs. A scan pair is regarded correctly-aligned if the average distance between the points under the estimated transformation (R_{pre}, t_{pre}) and these points under the ground truth transformation (R_{gt}, t_{gt}) is less than 0.2m for the 3D(Lo)Match dataset and 0.5m for the ETH dataset. RR of all methods is calculated on the same official evaluation scan pairs mentioned in Sec. 4.1.1.

For the evaluation on ScanNet, we follow [21, 30, 55] to report Empirical Cumulative Distribution Functions (ECDF) of the rotation error re and translation error te :

$$re = \arccos\left(\frac{\text{tr}(R_{pre}^T R_{gt}) - 1}{2}\right) \quad te = \|t_{pre} - t_{gt}\|^2. \quad (13)$$

We also report the number of required pairwise registrations to initialize the pose graphs, denoted as “#Pair”.

4.1.3 Baselines

We compare the proposed method against several multiview registration baselines: EIGSE3 [5], L1-IRLS [11], RotAvg [11], LMVR [21], LITS [55], and HARA [37]. Specifically, LMVR is an end-to-end method, which performs pairwise registration and transformation synchronization in a single deep neural network. EIGSE3 proposes a spectral approach to solve transformation synchronization and further applies IRLS with Cauchy [26] reweighting function to improve robustness. L1-IRLS and RotAvg are two robust algorithms, which perform IRLS-based rotation synchronization using l_1 and $l_{1/2}$ reweighting functions to resist outliers. HARA is a state-of-the-art hand-crafted synchronization method, which conducts growing-based edge pruning by checking cycle consistency and performs IRLS-based synchronization using $l_{1/2}$ reweighting functions on the retained edges. LITS is a state-of-the-art learning-based transformation synchronization method. All baseline methods except LMVR are compatible with any pairwise registration methods [1, 15, 46, 49]. Thus, we com-

Pose Graph	Method	#Pair	SpinNet [1] 3D / 3DL-RR (%)	YOHO [49] 3D / 3DL-RR (%)	GeoTrans [46] 3D / 3DL-RR (%)
Full	EIGSE3 [5]	11905	20.8 / 13.6	23.2 / 6.6	17.0 / 9.1
	L1-IRLS [11]	11905	49.8 / 29.4	52.2 / 32.2	55.7 / 37.3
	RotAvg [11]	11905	59.3 / 38.9	61.8 / 44.1	68.6 / 56.5
	LITS [55]	11905	68.1 / 47.9	77.0 / 59.0	84.2 / 73.0
	HARA [37]	11905	82.7 / 63.6	83.1 / 68.7	83.4 / 68.5
	Ours	11905	93.3 / 77.2	93.2 / 76.8	91.5 / 82.4
	Ours	11905	42.7 / 34.6	40.1 / 26.5	39.4 / 28.7
Pruned [21]	L1-IRLS [11]	11905	66.9 / 46.2	68.6 / 49.0	77.4 / 58.3
	RotAvg [11]	11905	72.8 / 55.3	77.2 / 60.3	81.6 / 68.5
	LITS [55]	11905	73.1 / 55.5	80.8 / 65.2	84.6 / 76.8
	HARA [37]	11905	84.0 / 62.5	83.8 / 71.9	84.9 / 73.7
	Ours	11905	94.8 / 80.6	95.2 / 82.3	95.2 / 82.8
	Ours	2798	94.9 / 80.0	96.2 / 81.6	95.9 / 83.0
	Ours	Ours	2798	94.9 / 80.0	96.2 / 81.6

Table 1. Registration recall on the 3DMatch (“3D”) and 3DLoMatch (“3DL”) datasets. We report results with different pairwise registration algorithms (SpinNet [1], YOHO [49], GeoTrans [46]).

pare our method with these baselines using different pairwise registration algorithms, including FCGF [15], SpinNet [1], YOHO [49], GeoTransformer [46].

4.1.4 Pose graph construction

For a fair comparison with baseline multiview registration methods, we report the performances produced on three different types of input pose graphs. The first type “Full” does not prune any edge so the pose graph is fully-connected. The second type “Pruned” prunes edges according to the quality of pairwise registration, which is adopted by previous methods LITS [55] and LMVR [21] (called “Good” in their papers). “Pruned” first applies pairwise registration algorithms (FCGF [15], YOHO [49], SpinNet [1] or GeoTransformer [46]) to exhaustively register all scan pairs and then only retain scan pairs whose median point distance in the registered overlapping region is less than 0.05m [21, 55] (0.15m for ETH). The final type “Ours” applies the proposed global feature for the overlap score estimation and constructs a sparse graph according to scores.

4.2. Results on three benchmarks

Qualitative results are shown in Fig. 4. Quantitative results on the 3DMatch, the ScanNet and the ETH datasets

Pose Graph	Method	#Pair	Rotation Error						Translation Error (m)					
			3°	5°	10°	30°	45°	Mean/Med	0.05	0.1	0.25	0.5	0.75	Mean/Med
Full	LMVR [21]	13920	48.3	53.6	58.9	63.2	64.0	48.1°/33.7°	34.5	49.1	58.5	61.6	63.9	0.83/0.55
	LITS [55]	13920	47.4	58.4	70.5	78.3	79.7	27.6°/-	29.6	47.5	66.7	73.3	77.6	0.56/-
	EIGSE3 [5]*	13920	19.7	24.4	32.3	49.3	56.9	53.6°/48.0°	11.2	19.7	30.5	45.7	56.7	1.03/0.94
	L1-IRLS [11]*	13920	38.1	44.2	48.8	55.7	56.5	53.9°/47.1°	18.5	30.4	40.7	47.8	54.4	1.14/1.07
	RotAvg [11]*	13920	44.1	49.8	52.8	56.5	57.3	53.1°/44.0°	28.2	40.8	48.6	51.9	56.1	1.13/1.05
	LITS [55]*	13920	52.8	67.1	74.9	77.9	79.5	26.8°/27.9°	29.4	51.1	68.9	75.0	77.0	0.68/0.66
	HARA [37]*	13920	54.9	64.3	71.3	74.1	74.2	32.1°/29.2°	35.8	54.4	66.3	69.7	72.9	0.87/0.75
	Ours	13920	57.2	68.5	75.1	78.1	78.8	26.4°/19.5°	39.4	61.5	72.0	75.2	77.6	0.70/0.59
Pruned [21]	EIGSE3 [5]*	13920	40.8	46.3	51.9	61.2	65.7	40.6°/37.1°	23.9	38.5	51.0	59.3	66.1	0.88/0.84
	L1-IRLS [11]*	13920	46.3	54.2	61.6	64.3	66.8	41.8°/34.0°	24.1	38.5	48.3	55.6	60.9	1.05/1.01
	RotAvg [11]*	13920	50.2	60.1	65.3	66.8	68.8	38.5°/31.6°	31.8	49.0	58.8	63.3	65.6	0.96/0.83
	LITS [55]*	13920	54.3	69.4	75.6	78.5	80.3	24.9°/19.9°	31.4	54.4	72.3	76.7	79.6	0.65/0.56
	HARA [37]*	13920	55.7	63.7	69.0	70.8	72.1	34.7°/31.3°	35.2	53.6	65.4	68.6	71.7	0.86/0.71
	Ours	13920	59.4	71.9	80.0	82.1	82.6	21.7°/19.1°	39.9	63.0	74.3	77.6	80.2	0.64/0.47
Ours	Ours	6004	59.1	73.1	80.8	82.5	83.0	21.7°/19.0°	39.9	64.1	76.7	79.0	81.9	0.56/0.49

* means using the same selected frames and pairwise transformations as ours.

Table 2. Registration performance on the ScanNet dataset. The pairwise registration algorithm for all methods is YOHO [49] except for LMVR [21] which includes pairwise registration in its pipeline.

Pose Graph	Method	#Pair	FCGF [15] RR (%)	SpinNet [1] RR (%)	YOHO [49] RR (%)
Full	EIGSE3 [5]	2123	44.8	56.3	60.9
	L1-IRLS [11]	2123	60.5	73.2	77.2
	RotAvg [11]	2123	67.3	82.1	85.4
	LITS [55]	2123	26.3	36.4	34.8
	HARA [37]	2123	72.2	79.3	85.4
	Ours	2123	85.7	86.3	98.8
	Ours	2123	89.4	93.6	96.3
Pruned [21]	L1-IRLS [11]	2123	86.1	87.9	90.2
	RotAvg [11]	2123	95.6	95.5	96.6
	LITS [55]	2123	41.2	47.3	48.4
	HARA [37]	2123	90.3	97.8	96.0
	Ours	2123	96.8	99.8	97.2
	Ours	Ours	516	97.4	99.8

Table 3. Registration recall on the ETH dataset. We report results using different pairwise registration algorithms (FCGF [15], SpinNet [1], YOHO [49]).

are shown in Table 1, Table 2 and Table 3, respectively.

First, the results show that our method achieves significant better performances than all baseline methods with $\sim 5\%$ - 10% improvements on the 3DMatch and 3DLoMatch dataset, which demonstrates that our method is able to accurately align low-overlapped scan pairs via pose synchronization. Meanwhile, our method only requires $\sim 30\%$ pairwise registrations with the help of our sparse graph construction, which greatly improves the efficiency.

Second, when using the same pose graphs as previous method, our method already achieves better performances on all datasets, which is benefited from our history reweighting function in the IRLS. Meanwhile, applying our global features for the graph construction further improves the results, which demonstrates the predicted overlap score is more robust than simply pruning edges according to the pairwise registration.

Finally, the results on the outdoor ETH dataset demon-

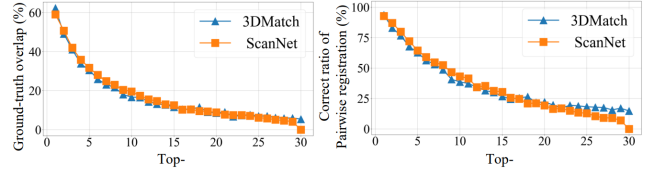


Figure 5. Ground truth overlap ratios and correct ratios of pairwise registration with Top-k overlap scores.

strate the generalization ability of the proposed method. Both our method and the learning-based method LITS [55] is trained on the indoor 3DMatch dataset, However, LITS does not generalize well to outdoor dataset (only $\sim 45\%$ recall) even though it shows strong performances on both indoor datasets. In comparison, our method still achieves strong performances (almost 100% registration recall) on the outdoor dataset.

4.3. Analysis

We thoroughly conduct analyses on the proposed designs about the pose graph construction and history reweighting IRLS modules in this section. By default, all analyses are conducted on the 3D(Lo)Match dataset with YOHO [49] as the pairwise registration method.

4.3.1 Sparse Graph Construction

Are predicted overlap scores well-calibrated? Well-calibrated overlap scores should assign higher scores to scan pairs with more overlap regions. Meanwhile, we want the scan pairs with higher overlap scores can be easily aligned by the pairwise registration algorithms. In Fig. 5, we report the averaged ground truth overlap ratios and correct ratio of pairwise registration of scan pairs with top-30 predicted overlap scores. It can be seen that the estimated overlap

Pose Graph	Method	#Pair	3D-RR (%)	3DL-RR (%)
Full	EIGSE3 [5]	11905	23.2	6.6
Pruned [21]	EIGSE3 [5]	11905	40.1	26.5
Ours	EIGSE3 [5]	2798	60.4	44.6
Full	RotAvg [11]	11905	61.8	44.1
Pruned [21]	RotAvg [11]	11905	77.2	60.3
Ours	RotAvg [11]	2798	81.7	63.9
Full	LITS [55]	11905	77.0	59.0
Pruned [21]	LITS [55]	11905	80.8	65.2
Ours	LITS [55]	2798	84.6	68.6

Table 4. Performances of applying different multiview registration methods on different input pose graphs.

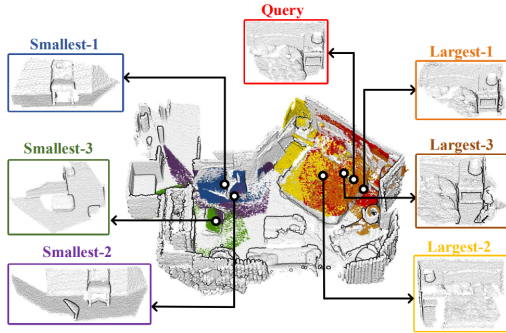


Figure 6. An example of retrieving scans using the global feature. The predicted top-3 scans with largest overlap scores indeed have large overlaps with the query scan while the 3 scans with smallest overlap scores are far away from the query.

scores are able to identify the reliable scan pairs with high overlap ratios. A visualization of retrieved scans using the global feature is given in Fig. 6.

Can our sparse graphs improve other multiview registration methods? We compare the performance of EIGSE3 [5], RotAvg [11], and LITS [55] using the fully-connected pose graph (“Full”), outliers pruned by pairwise registration results [21, 30, 55] (“Pruned”) and the proposed sparse graph (“Ours”) in Table 4. It can be seen that our sparse graph construction boosts the performance of baseline methods by a larger margin than “Pruned” graphs. Note “Pruned” requires exhaustive pairwise registration while we only need to conduct pairwise registration on the retained edges. Thus, our method is more efficient. Detailed running times are provided in the supplementary material.

4.3.2 Ablation studies on history reweighting

We conduct ablation studies on our designs in the proposed IRLS algorithm. The results are shown in Table 5 and the convergence curves are shown in Fig. 7. We consider the following three designs. 1) *Weight initialization (WI)*. We initialize the weight to be the product of both the inlier correspondence number r_{ij} and the predicted overlap score s_{ij} . Alternatively, we may just initialize the weight with r_{ij} or s_{ij} only. Results show that the proposed initialization

	Initialization		Reweighting		Full
	w/o s_{ij}	w/o r_{ij}	w/o HR	w/o INC	
3D-RR(%)	95.5 (-0.7)	76.9 (-19.3)	83.1 (-13.1)	94.1 (-2.1)	96.2
3DL-RR(%)	79.9 (-1.7)	63.4 (-18.2)	68.9 (-12.7)	79.8 (-1.8)	81.6

Table 5. Ablation studies on the proposed IRLS scheme.

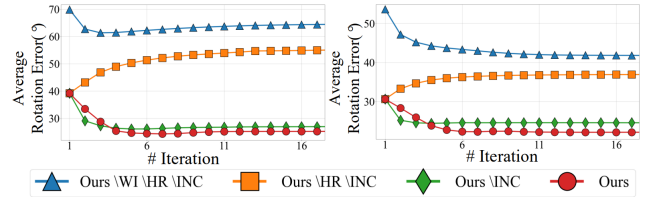


Figure 7. Curves of rotation error w.r.t. iteration number with ablation on specific components of our IRLS scheme on the 3DMatch (left) and the ScanNet (right). “\” means “without”.

is better. 2) *History reweighting (HR)*. In our reweighting function, the recomputed weight is determined by rotation residuals of all previous iterations. Alternatively, we may just compute the weight from the rotation residual of current iteration. History reweighting stabilizes the iterative refinement and makes IRLS more robust to outliers. 3) *Designing $g(m)$ to be increasing with m (INC)*. In our design, we set $g(m)$ to be increasing with m so that the residuals at early iterations will have smaller impacts on results. Alternatively, we may set $g(m) = 1/M$ so that all residuals contribute equally to the weights. However, rotations estimated in the early stage are not very stable so that reducing their impacts will improve the results.

5. Conclusion

In this paper, we propose a novel multiview point cloud registration method. The key of the proposed method is a learning-based sparse pose graph construction which can estimate a overlap ratio between two scans, enabling us to select high-overlap scan pairs to construct a sparse but reliable graph. Then, we propose a novel history reweighting function in IRLS scheme, which improves robustness to outliers and has better convergence to correct poses. The proposed method demonstrates the state-of-the-arts performances on both indoor and outdoor datasets with much fewer pairwise registrations.

6. Acknowledgement

This research is jointly sponsored by the National Key Research and Development Program of China (No.2022YFB3904102), the National Natural Science Foundation of China Projects (No.42171431, U20A20185, 61972435), the Open Fund of Hubei LuoJia Laboratory (No.2201000054) and the Guangdong Basic and Applied Basic Research Foundation (2022B1515020103).

References

- [1] Sheng Ao, Qingyong Hu, Bo Yang, Andrew Markham, and Yulan Guo. Spinnet: Learning a general surface descriptor for 3d point cloud registration. In *CVPR*, 2021. 1, 3, 5, 6, 7
- [2] Yasuhiro Aoki, Hunter Goforth, Rangaprasad Arun Srivatsan, and Simon Lucey. Pointnetlk: Robust & efficient point cloud registration using pointnet. In *CVPR*, 2019. 3
- [3] Relja Arandjelovic, Petr Gronat, Akihiko Torii, Tomas Pfajdla, and Josef Sivic. Netvlad: Cnn architecture for weakly supervised place recognition. *IEEE TPAMI*, 40(06):1437–1451, 2018. 3, 11
- [4] Mica Arie-Nachimson, Shahar Z Kovalsky, Ira Kemelmacher-Shlizerman, Amit Singer, and Ronen Basri. Global motion estimation from point matches. In *3DIMPVT*, 2012. 4, 11
- [5] Federica Arrigoni, Beatrice Rossi, and Andrea Fusiello. Spectral synchronization of multiple views in se (3). *SIAM Journal on Imaging Sciences*, 9(4):1963–1990, 2016. 2, 3, 5, 6, 7, 8
- [6] Xuyang Bai, Zixin Luo, Lei Zhou, Hongkai Chen, Lei Li, Zeyu Hu, Hongbo Fu, and Chiew-Lan Tai. Pointdsc: Robust point cloud registration using deep spatial consistency. In *CVPR*, 2021. 3
- [7] Xuyang Bai, Zixin Luo, Lei Zhou, Hongbo Fu, Long Quan, and Chiew-Lan Tai. D3feat: Joint learning of dense detection and description of 3d local features. In *CVPR*, 2020. 1, 3
- [8] Florian Bernard, Johan Thunberg, Peter Gemmar, Frank Hertel, Andreas Husch, and Jorge Goncalves. A solution for multi-alignment by transformation synchronisation. In *CVPR*, 2015. 3
- [9] Uttaran Bhattacharya and Venu Madhav Govindu. Efficient and robust registration on the 3d special euclidean group. In *ICCV*, 2019. 3
- [10] Tolga Birdal, Umut Simsekli, Mustafa Onur Eken, and Slobodan Ilic. Bayesian pose graph optimization via bingham distributions and tempered geodesic mcmc. *NeurIPS*, 2018. 3
- [11] Avishek Chatterjee and Venu Madhav Govindu. Robust relative rotation averaging. *IEEE TPAMI*, 40(4):958–972, 2017. 2, 6, 7, 8, 13, 14, 15, 16
- [12] Zhi Chen, Kun Sun, Fan Yang, and Wenbing Tao. Sc2-pcr: A second order spatial compatibility for efficient and robust point cloud registration. In *CVPR*, 2022. 3
- [13] Sungjoon Choi, Qian-Yi Zhou, and Vladlen Koltun. Robust reconstruction of indoor scenes. In *CVPR*, 2015. 2, 3
- [14] Christopher Choy, Wei Dong, and Vladlen Koltun. Deep global registration. In *CVPR*, 2020. 3
- [15] Christopher Choy, Jaesik Park, and Vladlen Koltun. Fully convolutional geometric features. In *ICCV*, 2019. 3, 5, 6, 7, 11
- [16] Angela Dai, Angel X Chang, Manolis Savva, Maciej Halber, Thomas Funkhouser, and Matthias Nießner. Scannet: Richly-annotated 3d reconstructions of indoor scenes. In *CVPR*, 2017. 3, 5
- [17] Zhen Dong, Fuxun Liang, Bisheng Yang, Yusheng Xu, Yufu Zang, Jianping Li, Yuan Wang, Wenxia Dai, Hongchao Fan, Juha Hyyppä, et al. Registration of large-scale terrestrial laser scanner point clouds: A review and benchmark. *ISPRS J*, 163:327–342, 2020. 1
- [18] Zhen Dong, Bisheng Yang, Fuxun Liang, Ronggang Huang, and Sebastian Scherer. Hierarchical registration of unordered tfs point clouds based on binary shape context descriptor. *ISPRS J*, 144:61–79, 2018. 1, 3
- [19] Mohamed El Banani, Ignacio Rocco, David Novotny, Andrea Vedaldi, Natalia Neverova, Justin Johnson, and Ben Graham. Self-supervised correspondence estimation via multiview registration. In *WACV*, 2023. 3, 12
- [20] Kexue Fu, Shaolei Liu, Xiaoyuan Luo, and Manning Wang. Robust point cloud registration framework based on deep graph matching. In *CVPR*, 2021. 3
- [21] Zan Gojcic, Caifa Zhou, Jan D Wegner, Leonidas J Guibas, and Tolga Birdal. Learning multiview 3d point cloud registration. In *CVPR*, 2020. 1, 2, 3, 4, 5, 6, 7, 8, 11, 13
- [22] Zan Gojcic, Caifa Zhou, Jan D Wegner, and Andreas Wieser. The perfect match: 3d point cloud matching with smoothed densities. In *CVPR*, 2019. 1, 3
- [23] Venu Madhav Govindu. Lie-algebraic averaging for globally consistent motion estimation. In *CVPR*, 2004. 3
- [24] Yulan Guo, Ferdous Sohel, Mohammed Bennamoun, Jianwei Wan, and Min Lu. An accurate and robust range image registration algorithm for 3d object modeling. *TMM*, 16(5):1377–1390, 2014. 3
- [25] Yulan Guo, Hanyun Wang, Qingyong Hu, Hao Liu, Li Liu, and Mohammed Bennamoun. Deep learning for 3d point clouds: A survey. *IEEE TPAMI*, 43(12):4338–4364, 2020. 1
- [26] Paul W Holland and Roy E Welsch. Robust regression using iteratively reweighted least-squares. *Communications in Statistics-theory and Methods*, 6(9):813–827, 1977. 3, 6
- [27] Qingyong Hu, Bo Yang, Linhai Xie, Stefano Rosa, Yulan Guo, Zhihua Wang, Niki Trigoni, and Andrew Markham. Randa-net: Efficient semantic segmentation of large-scale point clouds. In *CVPR*, 2020. 1
- [28] Shengyu Huang, Zan Gojcic, Mikhail Usvyatsov, Andreas Wieser, and Konrad Schindler. Predator: Registration of 3d point clouds with low overlap. In *CVPR*, 2021. 1, 3, 5, 12
- [29] Xiangru Huang, Zhenxiao Liang, Chandrajit Bajaj, and Qixing Huang. Translation synchronization via truncated least squares. *NeurIPS*, 2017. 2, 3, 11
- [30] Xiangru Huang, Zhenxiao Liang, Xiaowei Zhou, Yao Xie, Leonidas J Guibas, and Qixing Huang. Learning transformation synchronization. In *CVPR*, 2019. 1, 2, 3, 4, 5, 6, 8, 11
- [31] Xiaoshui Huang, Guofeng Mei, and Jian Zhang. Feature-metric registration: A fast semi-supervised approach for robust point cloud registration without correspondences. In *CVPR*, 2020. 3
- [32] Xiaoshui Huang, Guofeng Mei, Jian Zhang, and Rana Abbas. A comprehensive survey on point cloud registration. *arXiv preprint arXiv:2103.02690*, 2021. 1
- [33] Daniel F Huber and Martial Hebert. Fully automatic registration of multiple 3d data sets. *Image and Vision Computing*, 21(7):637–650, 2003. 3

- [34] Diederik P Kingma and Jimmy Ba. Adam: A method for stochastic optimization. *arXiv preprint arXiv:1412.6980*, 2014. 5
- [35] Loic Landrieu and Martin Simonovsky. Large-scale point cloud semantic segmentation with superpoint graphs. In *CVPR*, 2018. 1
- [36] Junha Lee, Seungwook Kim, Minsu Cho, and Jaesik Park. Deep hough voting for robust global registration. In *ICCV*, 2021. 3
- [37] Seong Hun Lee and Javier Civera. Hara: A hierarchical approach for robust rotation averaging. In *CVPR*, 2022. 6, 7, 13, 14, 15, 16
- [38] Xueqian Li, Jhony Kaesemodel Pontes, and Simon Lucey. Deterministic pointnetlk for generalized registration. *arXiv preprint arXiv:2008.09527*, 2020. 3
- [39] Yang Li and Tatsuya Harada. Leopard: Learning partial point cloud matching in rigid and deformable scenes. In *CVPR*, 2022. 1, 3
- [40] Weixin Lu, Guowei Wan, Yao Zhou, Xiangyu Fu, Pengfei Yuan, and Shiyu Song. Deepvcv: An end-to-end deep neural network for point cloud registration. In *ICCV*, 2019. 3
- [41] Daniel Martinec and Tomas Pajdla. Robust rotation and translation estimation in multiview reconstruction. In *CVPR*, 2007. 11
- [42] Ajmal S Mian, Mohammed Bennamoun, and Robyn Owens. Three-dimensional model-based object recognition and segmentation in cluttered scenes. *IEEE TPAMI*, 28(10):1584–1601, 2006. 3
- [43] G Dias Pais, Srikumar Ramalingam, Venu Madhav Govindu, Jacinto C Nascimento, Rama Chellappa, and Pedro Miraldo. 3dregnet: A deep neural network for 3d point registration. In *CVPR*, 2020. 3
- [44] François Pomerleau, Ming Liu, Francis Colas, and Roland Siegwart. Challenging data sets for point cloud registration algorithms. In *IJRR*, 2012. 3, 5
- [45] Charles R Qi, Hao Su, Kaichun Mo, and Leonidas J Guibas. Pointnet: Deep learning on point sets for 3d classification and segmentation. In *CVPR*, 2017. 3
- [46] Zheng Qin, Hao Yu, Changjian Wang, Yulan Guo, Yuxing Peng, and Kai Xu. Geometric transformer for fast and robust point cloud registration. In *CVPR*, 2022. 1, 3, 5, 6
- [47] Pascal Willy Theiler, Jan Dirk Wegner, and Konrad Schindler. Globally consistent registration of terrestrial laser scans via graph optimization. *ISPRS J*, 109:126–138, 2015. 3
- [48] Andrea Torsello, Emanuele Rodola, and Andrea Albarelli. Multiview registration via graph diffusion of dual quaternions. In *CVPR*, 2011. 3
- [49] Haiping Wang, Yuan Liu, Zhen Dong, and Wenping Wang. You only hypothesize once: Point cloud registration with rotation-equivariant descriptors. In *ACM Multimedia*, 2022. 1, 3, 4, 5, 6, 7, 11, 12
- [50] Haiping Wang, Yuan Liu, Qingyong Hu, Bing Wang, Jianguo Chen, Zhen Dong, Yulan Guo, Wenping Wang, and Bisheng Yang. Roreg: Pairwise point cloud registration with oriented descriptors and local rotations. *IEEE TPAMI*, 2023. 3
- [51] Yue Wang and Justin M Solomon. Deep closest point: Learning representations for point cloud registration. In *CVPR*, 2019. 3
- [52] Yue Wang and Justin M Solomon. Prnet: Self-supervised learning for partial-to-partial registration. In *NeurIPS*, 2019. 3
- [53] Hao Wu, Li Yan, Hong Xie, Pengcheng Wei, and Jicheng Dai. A hierarchical multiview registration framework of the point clouds based on loop constraint. *ISPRS J*, 2023. 3, 12
- [54] Bisheng Yang, Zhen Dong, Fuxun Liang, and Yuan Liu. Automatic registration of large-scale urban scene point clouds based on semantic feature points. *ISPRS J*, 113:43–58, 2016. 1
- [55] Zi Jian Yew and Gim Hee Lee. Learning iterative robust transformation synchronization. In *3DV*, 2021. 1, 2, 3, 4, 5, 6, 7, 8, 13, 14, 15, 16
- [56] Zi Jian Yew and Gim Hee Lee. Regtr: End-to-end point cloud correspondences with transformers. In *CVPR*, 2022. 3
- [57] Hao Yu, Fu Li, Mahdi Saleh, Benjamin Busam, and Slobodan Ilic. Cofinet: Reliable coarse-to-fine correspondences for robust pointcloud registration. *NeurIPS*, 2021. 1, 3
- [58] Wentao Yuan, Benjamin Eckart, Kihwan Kim, Varun Jampani, Dieter Fox, and Jan Kautz. Deepgmr: Learning latent gaussian mixture models for registration. In *ECCV*, 2020. 3
- [59] Andy Zeng, Shuran Song, Matthias Nießner, Matthew Fisher, Jianxiong Xiao, and Thomas Funkhouser. 3dmatch: Learning local geometric descriptors from rgb-d reconstructions. In *CVPR*, 2017. 3, 5, 12
- [60] Qian-Yi Zhou, Jaesik Park, and Vladlen Koltun. Fast global registration. In *ECCV*, 2016. 3, 4

7. Appendix

In this supplementary material, we provide the detailed solution of pose synchronization in Sec. A.1, the implementation details in Sec. A.2, additional analysis in Sec. A.3, the running time analysis in Sec. A.4, and more qualitative results in Sec. A.6.

A.1. Pose synchronization

In this section, we provide the detailed solution of pose synchronization in Sec. 3.3.2 of the main paper. Given the edge weights and input relative poses $\{w_{ij}, T_{ij} | (i, j) \in \mathcal{E}\}$, we solve the transformation synchronization by dividing it into rotation synchronization [4, 30] and translation synchronization [29]. In the following, our pairwise transformation $T_{ij} = (R_{ij}, t_{ij})$ on edge $(i, j) \in \mathcal{E}$ aligns the source scan P_j to the target scan P_i . The scan poses are assumed to be camera-to-world matrices. Thus scans under the correctly recovered poses $\{(R_i, t_i)\}$ should reconstruct the whole scenario.

Rotation synchronization. Following [4, 21, 41], we treat the synchronization of rotations $\{R_i\}$ as an over-constrained optimization problem:

$$\arg \min_{R_1, \dots, R_N \in SO(3)} \sum_{(i,j) \in \mathcal{E}} w_{ij} \|R_{ij} - R_i^T R_j\|_F^2, \quad (\text{A.1})$$

where $\|\cdot\|_F$ means the Frobenius norm of the matrix. Under the spectral relaxation, a closed-form solution of Eq. A.1 can be computed as follows [4, 21]. Consider a symmetric matrix $L \in \mathbb{R}^{3N \times 3N}$ containing $N^2 3 \times 3$ blocks:

$$L = \begin{pmatrix} \sum_{(1,j) \in \mathcal{E}} w_{1j} \mathbf{I}_3 & -w_{12} R_{12} & \cdots & -w_{1N} R_{1N} \\ -w_{21} R_{21} & \sum_{(2,j) \in \mathcal{E}} w_{2j} \mathbf{I}_3 & \cdots & -w_{2N} R_{2N} \\ \vdots & \vdots & \ddots & \vdots \\ -w_{N1} R_{N1} & -w_{N2} R_{N2} & \cdots & \sum_{(N,j) \in \mathcal{E}} w_{Nj} \mathbf{I}_3 \end{pmatrix}, \quad (\text{A.2})$$

where $\mathbf{I}_3 \in \mathbb{R}^{3 \times 3}$ denotes the identity matrix. For each edge $(i, j) \in \mathcal{E}$, we fill $-w_{ij} R_{ij}$ and $-w_{ij} R_{ij}^T$ to the (i, j) and (j, i) block. For unconnected edges, we set the corresponding blocks to zeros.

We first calculate three eigenvectors $\tau_1, \tau_2, \tau_3 \in \mathbb{R}^{3N}$ corresponding to the three smallest eigenvalues $\lambda_1 < \lambda_2 < \lambda_3$ of L and stack them to form $\gamma = [\tau_1, \tau_2, \tau_3] \in \mathbb{R}^{3N \times 3}$. Then, $v_i = \gamma[3i - 3 : 3i] \in \mathbb{R}^{3 \times 3}$ is an approximation of the absolute rotation R_i for point cloud P_i but may not satisfy the constraint $v_i v_i^T = \mathbf{I}_3$. Therefore, we rectify this by applying singular value decomposition on v_i by $v_i = U_i \sum_i V_i^T$ and deriving $R_i = V_i U_i^T$ [4]. Then, we further check $\det(R_i)$ and exchange the first two rows of R_i if $\det(R_i) = -1$.

Translation synchronization. Translation synchronization retrieves the translation vectors $\{t_i\}$ that minimize the

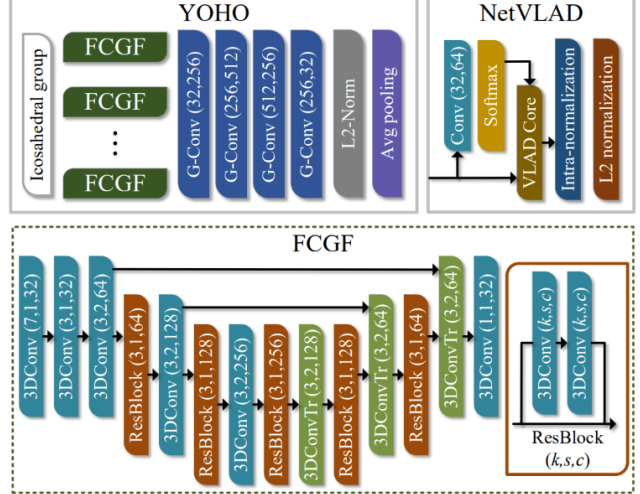


Figure A.1. Network architecture for global feature extraction. “G-Conv” means group convolution defined on Icosahedral group same as [49]. “VLAD core” is the same as [3]. For FCGF [15], “3DConv” and “3DConvTr” denotes a sparse convolution layer and the transpose convolution layer for upsampling, respectively.

problem:

$$\arg \min_{t_1, \dots, t_N \in \mathbb{R}^3} \sum_{(i,j) \in \mathcal{E}} w_{ij} \|R_i t_{ij} - t_j + t_i\|^2. \quad (\text{A.3})$$

We solve it by the standard least square method [29].

Assuming E edges are connected in \mathcal{G} , we thus construct three matrices A , B , and H as follows. $A \in \mathbb{R}^{3E \times 3E}$ is initialized as an identity matrix. $B \in \mathbb{R}^{3E \times 3N}$ contains $E * N 3 \times 3$ blocks and is initialized as a zero matrix. $H \in \mathbb{R}^{3E \times 1}$ is a vector containing $E 3 \times 1$ blocks. For the e -th edge $(i, j) \in \mathcal{E}$, we multiply $A[3e - 3 : 3e]$ with w_{ij} , fill \mathbf{I}_3 and $-\mathbf{I}_3$ to the (e, j) and (e, i) block of B respectively, and fill $R_i t_{ij}$ to the e -th block of H . We thus solve $t = (B^T A B)^{-1} B^T A H$ and obtain the translation vector t_i of each scan P_i as $t[3i - 3 : 3i]$.

A.2. Implementation details

A.2.1 Architecture

The architecture of our global feature extraction network is shown in Fig. A.1. We adopt YOHO with the same architecture as [49] for 32-dim local feature extraction. More local feature extraction details can be found in [49]. The extracted local features are aggregated to a global feature by a *NetVLAD* layer [3]. We set the number of clusters in *NetVLAD* to 64 and the dimension of the global feature is thus 2048. Please refer to [3] for more global feature aggregation details.

Overlap Estimation	3D-RR(%)	3DLo-RR(%)
Predator [28]	95.2	78.4
Ours	96.2	81.6

Table A.1. Registration recall on 3D(Lo)Match using estimated overlap scores from Predator [28] and ours.

A.2.2 Training details

We use the pretrained YOHO [49] for local feature extraction and train the *NetVLAD* layer using the 46 scenes in the training split of 3DMatch [59]. We adopt the following data augmentations. For each scene in the train set of 3DMatch, we first randomly sample $\alpha \in [8, 60]$ scans as the graph node. Then, on each scan, we randomly sample $\beta \in [1024, 5000]$ keypoints to extract YOHO features. The local features of α scans are fed to *NetVLAD* to extract α scan global features. Then, we compute the $\binom{\alpha}{2}$ overlap scores by exhaustively correlating every two global features and compute the L1 distance between the ground-truth overlap ratios and the predicted overlap scores as the loss for training. We set the batch size to 1 and use the Adam optimizer with a learning rate of 1e-3. The learning rate is exponentially decayed by a factor of 0.7 every 50 epoch. In total, we train the *NetVLAD* for 300 epochs.

A.3. More analysis

A.3.1 Use Predator [28] for overlap estimation

In Table. A.1, we use the overlap scores predicted by Predator [28] in the sparse graph construction, which yields slightly worse results. Moreover, Predator [28] applies cross-attention layers between local features of a scan pair to estimate overlap while we only need to compute a global feature for every scan and efficiently correlate the global features to estimate overlap. In our test, the proposed method is $10\times$ more efficient than Predator.

A.3.2 Concurrent multiview registration works

After our submission to CVPR 2023, two concurrent multiview registration works are available online, namely, SynMatch [19] and HL-MRF [53]. SynMatch and HL-MRF are specifically designed for registering raw RGB-D sequences and TLS point clouds, respectively, while the proposed method offering a more general approach. In our test, the proposed method notably outperforms SynMatch by 27% on the 3DMatch dataset. HL-MRF indeed performs well on the TLS-based ETH dataset but fails on the indoor datasets.

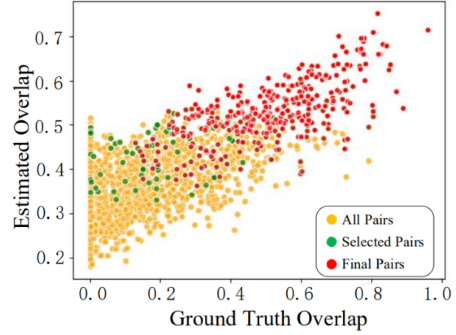


Figure A.2. Estimated overlap ratio versus the ground truth overlap ratio on scan pairs of the *Kitchen* scene of 3DMatch. “All pairs” means all $\binom{N}{2}$ scan pairs. “Selected pairs” means the scan pairs selected to construct the sparse pose graph. “Final pairs” means the scan pairs with an edge weight greater than 10^{-2} after transformation synchronization.

Top-	4	6	8	10	12	15	Full
# Pair	1167	1707	2250	2798	3349	4129	11905
Sync-time (s)	20.2	30.4	37.4	54.8	66.6	90.3	405.4
3D-RR (%)	91.3	91.6	95.5	96.2	96.6	96.0	93.2
3DL-RR (%)	71.0	74.7	80.9	81.6	81.2	80.3	76.8

Table A.2. Ablation study on k in sparse graph construction. “Full” means using fully-connected graphs. “Sync-time” means the time for transformation synchronization.

A.3.3 Estimated overlap versus ground truth overlap

In Fig. A.2, each point (o_{gt}, o_{est}) represents a scan pair with the ground truth overlap ratio o_{gt} and estimated overlap ratio o_{est} . The plot reveals several observations: (1) scan pairs with larger ground truth overlaps indeed have larger overlap scores; (2) the constructed sparse graph mainly contains scan pairs with higher overlap ratios, as evidenced by the green and red points; (3) the proposed transformation synchronization algorithm further eliminates unreliable scan pairs effectively to achieve accurate scan poses, as shown by the red points.

A.3.4 Use different top- k in sparse graph construction

In Table. A.2, we show the results with different k in the sparse graph construction. Retaining too many scan pairs with larger k may include more outliers while using too small k could split the whole graph into several disconnected subgraphs. Results show that using $k = 10$ or 12 brings the best results.

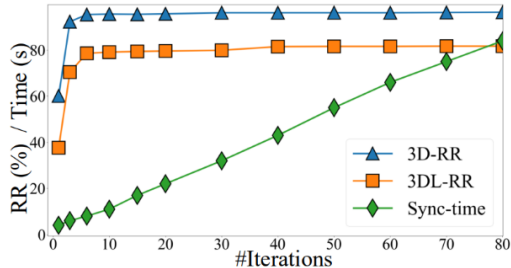


Figure A.3. Results of the proposed history reweighting IRLS with different iterations.

Method	Graph Cons (s)	Trans Sync (s)	Total (s)
RotAvg [11] + Full	86.3	49.4	135.7
LITS [55] + Full	86.3	0.7	87.0
HARA [37] + Full	87.3	8.5	95.8
RotAvg [11] + Pruned [21]	164.1	22.6	186.7
LITS [55] + Pruned [21]	164.1	0.7	164.8
HARA [37] + Pruned [21]	164.8	7.5	172.4
Ours	20.0	6.9	26.8

Table A.3. Detailed time consumption for registering a scene on 3DMatch. “Graph Cons” means the time for constructing the input pose graph. “Trans Sync” means the time for IRLS-based transformation synchronization.

A.3.5 Performances using different IRLS iterations

In Fig. A.3, we show the registration performance on 3D(Lo)Match with different iteration numbers. It can be seen that the results will be better with more iterations. However, using more iterations also costs more time. We thus select 50 iterations for its stable performance and efficiency by default.

A.4. Runtime analysis

In Table. A.3, we provide the runtime for the graph construction and the IRLS-based transformation synchronization averaged on the 8 scenes of the 3DMatch dataset. We evaluate the runtimes on a computer with Intel(R) Core(TM) i7-10700 CPU@ 2.90GHz with GeForce GTX 2080Ti and 64 GB RAM. Our sparse pose graph construction is nearly 67s faster than baselines for conducting much fewer pairwise registrations. In total, our method is 61s ~ 160s faster than baselines for registering a scene in 3DMatch.

A.5. Limitations

When the overlap ratios of two scans are too small and there are no other scans which forms a cycle with these two scans, our method may fail in this case. A typical example is shown in Fig. A.4, where overlap region in the red rectangle is very small and mainly consists of feature-less planar points. In this case, our method fails to register the whole



Figure A.4. A failure case in ScanNet. (a) The ground truth multiview registration (30 scans). (b) The multiview registration from the proposed method.

scene but separately recover poses on two subgraphs. This also shows that our method may have the potential to automatically separate scans from two different scenes, which is beyond the discussion of this paper.

A.6. More qualitative results

We provide additional qualitative results including success cases (Fig. A.5 and Fig. A.6) and failure cases (Fig. A.7). We also compare our results with the registration results of RotAvg [11], HARA [37], and LITS [55]. The failure of our method occurs when some overlap regions mainly contain the repetitive structures (top of Fig. A.7) or feature-less regions (bottom of Fig. A.7).

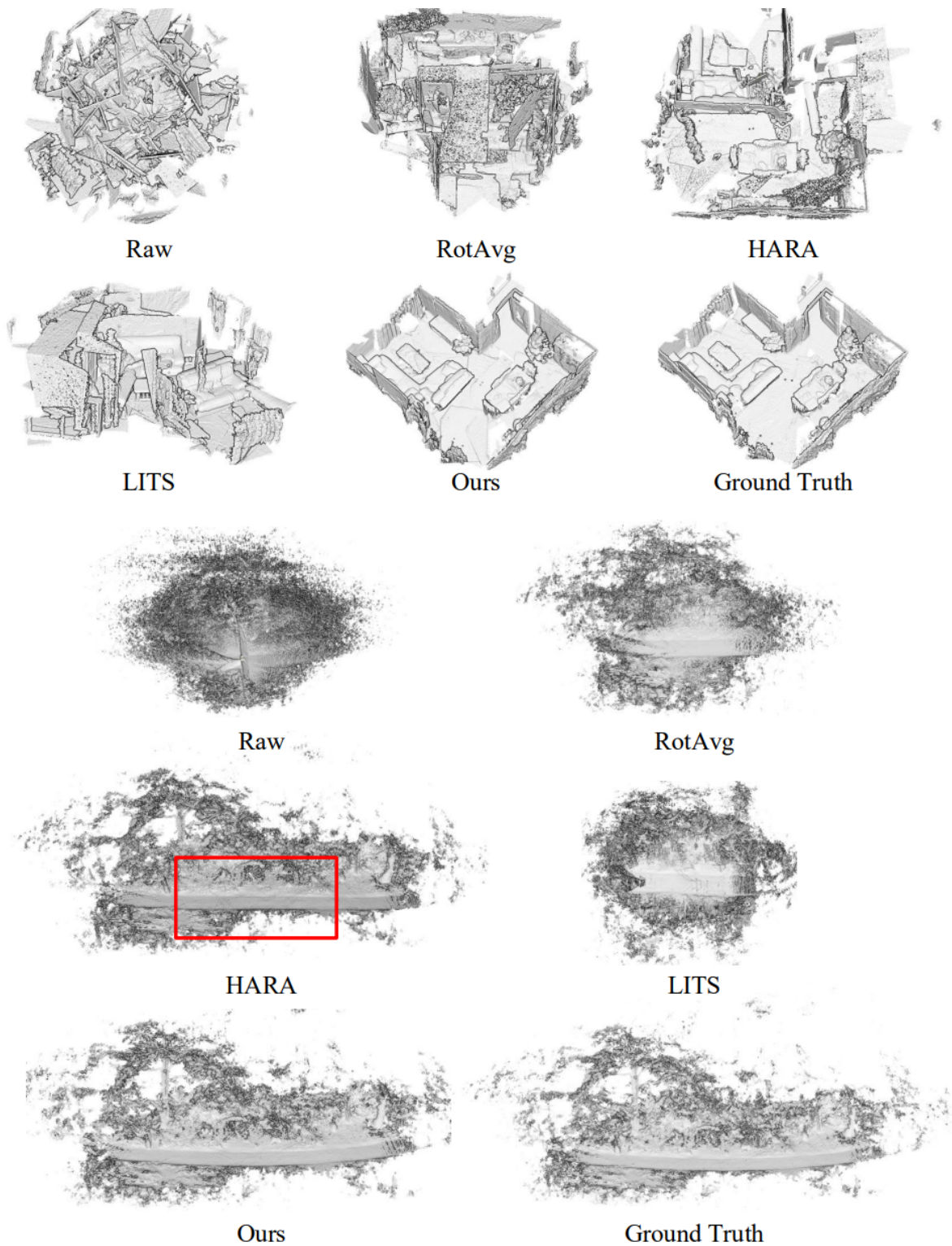


Figure A.5. Registration results of our method, RotAvg [11], HARA [37], and LITS [55] on the 3DMatch dataset and the ETH dataset. Top: the *Home1* scene of 3DMatch. Bottom: the *Wood_Summer* scene of ETH.

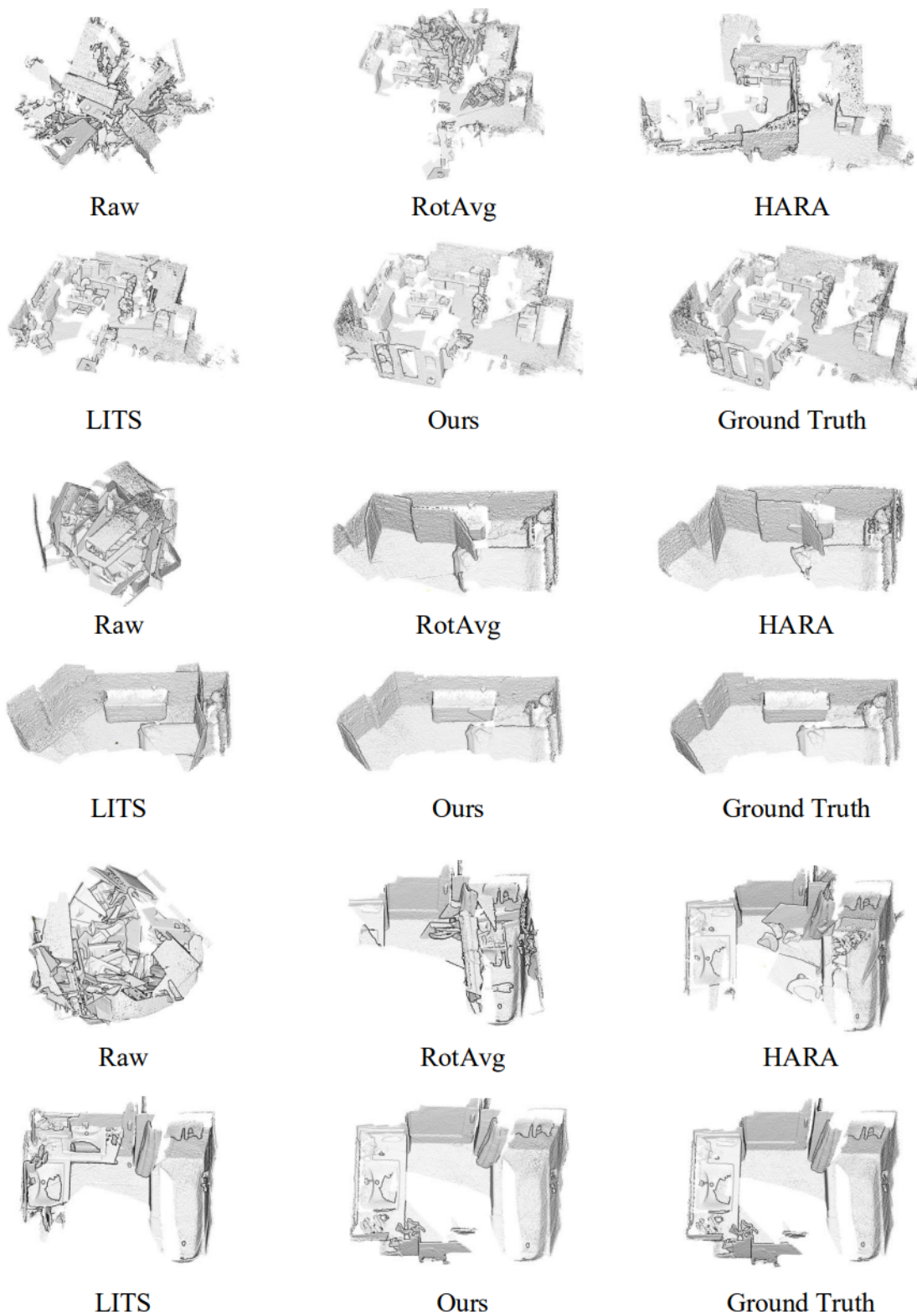


Figure A.6. Registration results of our method, RotAvg [11], HARA [37], and LITS [55] on scenes of ScanNet dataset including *Scene0309_00* (top), *Scene0286_02* (middle), and *Scene0265_02* (bottom).

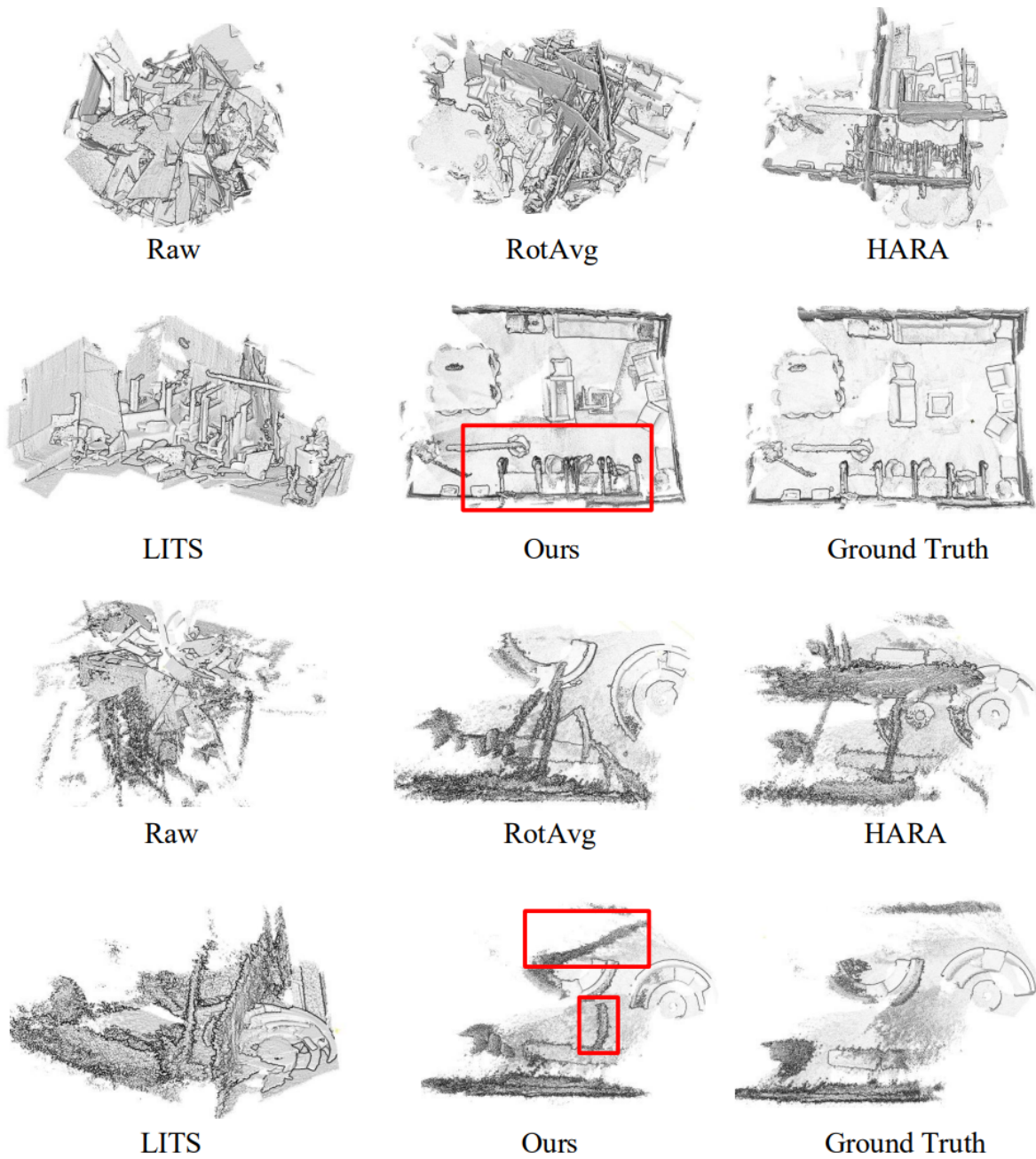


Figure A.7. Registration results of our method, RotAvg [11], HARA [37], and LITS [55] on 3DMatch (top: *Studyroom*) and ScanNet (bottom: *Scene0334_02*). Our method fails to register the scans in the red boxes due to repetitive structures and feature-less regions.